ELSEVIER

Improvement of sub-threshold current models for a-Si:H thin-film transistors

Lijuan Wang [a,*], Jiang Zhu [a], Chunling Liu [a], Guojun Liu [a], Xibin Shao [b], Donghang Yan [c]

[a] *State Key Laboratory of High Power Semiconductor Lasers, Changchun University of Science and Technology, Changchun 130022, People's Republic of China*
[b] *Changchun Institute of Optics, Fine Mechanics and Physics, Chinese Academy of Sciences, Changchun 130033, People's Republic of China*
[c] *State Key Laboratory of Polymer Physics and Chemistry, Changchun Institute of Applied Chemistry, Chinese Academy of Sciences, Changchun 130022, People's Republic of China*

Abstract

The improved sub-threshold drain–source current models of a-Si:H thin-film transistors (TFTs) is demonstrated in this paper. The current–voltage (I–V) characteristics of a-Si:H TFTs are revealed in both forward and reverse sub-threshold region. The I–V characteristics exhibit a strong dependence on the gate–source voltage (V_{GS}) and the drain–source voltage (V_{DS}). The effects of weak electron distribution and a lateral component of the electric field on the a-Si:H TFT characteristics, which are induced by V_{DS} at both front and back interface, are considered in current model. This strong dependence of the sub-threshold current on V_{DS} is attributed to the channel length, drain–gate overlap vicinity, and process condition. Simulated results based on the model exhibit a good agreement with measured experimental data. The proposed model and the modeling process will be very useful for practical TFTs simulation.
© 2007 Elsevier Ltd. All rights reserved.

Keywords: a-Si:H TFT; Model; Sub-threshold; Drain–source voltage

1. Introduction

Hydrogenated amorphous silicon thin-film transistors (a-Si:H TFTs) have been widely used for large area active matrix imaging systems [1] and liquid-crystal displays (AMLCD) [2]. Currently, the performances of the devices are often limited because of the sub-threshold leakage current of a-Si:H TFTs, which generally determines the on/off ratio of devices.

In several papers the weak accumulation of electrons changes through V_{DS} in the reverse sub-threshold region [6,8,10], the drain–source current varies exponentially with the gate–source voltage [5,6,8] in the forward sub-threshold region. However, with the development of a-Si:H TFTs, it is necessary that the sub-threshold current models should be elaborately studied. It is crucial to active matrix designers to evaluate and predict the performance of a-Si:H TFTs array.

In this paper, the analysis on the simulated results of the sub-threshold current model for a-Si:H TFTs has been done to confirm that the profile of electrons and a lateral component of electric field owing to V_{DS} are the main factors in determining the forward and reverse sub-threshold current, which are identical with the densities of the interface states and the deep localized states [7,9,11].

2. Experiment

The inverted-stagger structure of a-Si:H TFTs of the back channel stopped types is shown in Fig. 1. MoW film was deposited by sputtering on the substrate of glass.

---
* Corresponding author. Tel.: +86 043185262268.
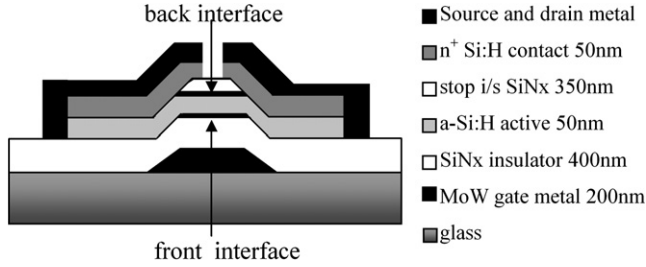*E-mail addresses:* osc3@ciac.jl.cn, wlj15@163.com (L. Wang).

Fig. 1. Cross-section of the a-Si: H TFT structure showing its different layer.

The layers of insulator SiN_x, a-Si:H and stop SiN_x were sequentially deposited by plasma enhanced chemical vapor deposition (PECVD). An n^+ a-Si was also deposited by PECVD. Ultimately, the Mo/AL/Mo were sputtered as drain and source electrodes. The drain–gate overlap length (ΔL) was 1 μm and the ratio of device width (W) and length (L) was $W/L = 26$ μm/11 μm. The characteristics were measured by using the Aglient 4155C at the room temperature.

3. Results and discussion

Fig. 2 depicts the transfer characteristics of the a-Si:H TFTs. Here, the sub-threshold region is identified from the off voltage (V_{TR}) to the threshold voltage (V_{TH}), which consists of the forward sub-threshold region from 0 V to V_{TH} and the reverse sub-threshold region from V_{TR} to 0 V. The two regions are characterized by conduction at the front interface and at the back interface [8], respectively.

In the forward and reverse sub-threshold region, the properties of TFTs varied exponentially with V_{DS} in this paper and differ from those in Refs. [8,6]. Both of the input–output characteristics curve of "$V_{GS} = 0$ V" and "$V_{GS} = 2$ V" also confirm the uniform exponential correlation with V_{DS}, as shown in Fig. 3 (solid lines). Due to the device geometry and process conditions, it is necessary to take into account the profile of electrons at the front interface and the back interface and a lateral component induced by V_{DS}. Based on some references in this section, the improved models are developed for the forward and reverse sub-threshold current, respectively.

3.1. Sub-threshold current models of some references

Kuo[6] has developed models for the conduction of the front interface in the forward sub-threshold region as the following:

$$I_{DS}^{subf} = \frac{W}{L} \cdot I_{sub0} \cdot \left[\exp\left(\frac{V'_{GS} - V_{TS}}{S_f} \right) - \exp\left(\frac{V'_{GD} - V_{TS}}{S_f} \right) \right] \tag{1}$$

Here, I_{DS}^{subf} is the drain–source current of the forward sub-threshold region, I_{sub0} is the current magnitude, and S_f is the forward sub-threshold slope. S_f and I_{sub0} can be ex-
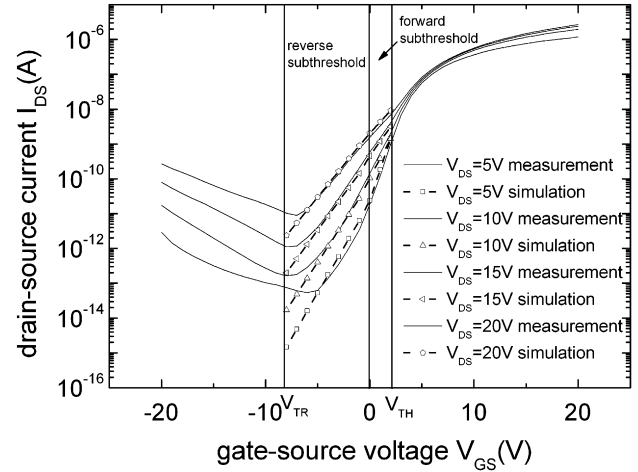

Fig. 2. Transfer characteristic curve of the forward and reverse sub-threshold regions simulated by improved model (11) and (12). The lines show the measured data; and the hollow makers and dotted lines show the simulated data.
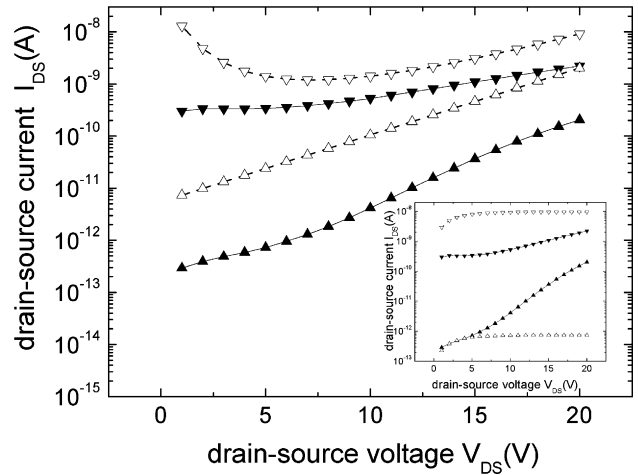

Fig. 3. Input–output characteristic curve of forward sub-threshold region simulated by improved model (11). The solid markers and lines show the measured data; and the hollow makers and dotted lines show the simulated data. From top to bottom, $V_{GS} = 0$ V, 2 V, respectively. Inset: the output characteristic curve of forward sub-threshold region simulated by Eq. (1).

tracted from the measured data. V_{TS} is the border of the forward sub-threshold region. V'_{GS} and V'_{GD} are the primed voltages affected by the contact resistances.

A model for the conduction of the back interface in the reverse sub-threshold region can be written as the following: [8,6]

$$I_{DS}^{subr} = \frac{W}{L} \cdot I_{rsub0} \cdot \exp\left(\frac{V'_{GS} - V_{TR}}{S_r + r_{rr}|V_{DS}|} \right) \tag{2}$$

Here I_{DS}^{subr} is the drain–source current in the reverse sub-threshold region, I_{rsub0} is the current magnitude, S_r is the reverse sub-threshold slope, r_{rr} is the fitting parameter affected by V_{DS}, V_{TR} is the threshold voltage of the reverse sub-threshold region.

3.2. Improved sub-threshold current models

Based on the above models, improved forward and reverse sub-threshold current models are presented in this paper. The two aspects are considered at the front and back interface respectively.

The inset of Fig. 4 shows that the simulated data by Eq. (1) are almost identical in the different drain–source voltage (V_{DS}). Hence, the effects of V_{DS} on the band bending ψ_{sf} at the front interface are neglected.

But the effects of V_{DS} on the current are very large in the measured data, as shown in Figs. 4 and 3 (solid lines). Therefore, it is important that the effect of V_{DS} on the forward sub-threshold current be considered from the two aspects.

This is the first factor. On account of the two-dimensional (2-D) nature of the boundary conditions at the drain–gate overlap vicinity, the electric field is no longer normal to the interface. It has a lateral component, and is a function of V_{DS}. Therefore, the electric field of Ref. [6] can be rewritten as the following:

$$\varepsilon(E_0 + \gamma V_{DS}) = qt_{si}n_{di}\exp(\psi_{sf}/V_{nd}) \tag{3}$$

Here, E_0 is the electric field at front interface, ε is the a-Si:H permittivity, t_{si} is the a-Si:H layer thickness, n_{di} the intrinsic electron density in the deep states, V_{nd} is the exponential slope of deep state electrons, q is the elementary charge, γ is the fitting parameter. Depending on the gate bias voltage, the term εE_0 denotes the charge in the a-Si:H semiconductor layer per unit area, which includes free carriers and charge trapped in the localized deep or tail states over the thickness of the a-Si:H layer[6]. Furthermore, $\varepsilon\gamma\, V_{DS}$ is the changed charge due to a lateral component of V_{DS} in this paper. The total channel charge should be induced under the two electric field of E_0 and a lateral component of V_{DS} together. The lateral component is induced by the two-dimensional nature of the boundary conditions at the drain overlap vicinity [6,8]. The Eq. (3) may be rewritten as

$$\varepsilon E_0 = qt_{si}n_{di}\exp(\psi_{sf}/V_{nd}) - \varepsilon\gamma V_{DS} \tag{4}$$

Substituting εE_0 from (4) into the deduction of Kuo [6], will yield the following:

$$V_{GS} - V_{ch} + \frac{\varepsilon\gamma}{C_i}V_{DS} - V_{TS} = x_n\psi_{sf} \tag{5}$$

Here, V_{ch} is the channel voltage, C_i is the insulator capacitance, x_n is the fitting parameter. Based on Ref. [8], the current may be reduced to the following:

$$I_{DS} = W\frac{dV_{ch}}{dx}q\mu_n n_{fi}\exp(\psi_{sf}/v_t)t_{si} \tag{6}$$

Here, v_t is the thermal voltage, n_{fi} is the intrinsic electron density, μ_n is the mobility. Substituting for the surface band bending ψ_{sf} from Eqs. (5) into (6), and integrating from source to drain yield the following:

$$I_{DS}^{subf} = \frac{W}{L}\cdot I_{sub0}\cdot\left[\exp\left(\frac{V'_{GS} - V_{TS} + \frac{\varepsilon\gamma}{C_i}V_{DS}}{S_f}\right)\right.$$
$$\left. - \exp\left(\frac{V'_{GD} - V_{TS} + \frac{\varepsilon\gamma}{C_i}V_{DS}}{S_f}\right)\right] \tag{7}$$

Because the effect of the source or drain contact resistance of 22.9 KΩ [6] on the sub-threshold current may be negligible, the Eq. (7) may be rewritten as

$$I_{DS}^{subf} = \frac{W}{L}\cdot I_{sub0}\cdot\exp\left(\frac{V_{GS} - V_{TS}}{S_f} + \frac{\varepsilon\gamma}{C_iS_f}V_{DS}\right)$$
$$\times\left[1 - \exp\left(-\frac{V_{DS}}{S_f}\right)\right] \tag{8}$$

The S_f of a-Si:H TFTs is below 1 V/dec [6], and V_{DS} is above 5 V, this implies that the factor $\left[1 - \exp\left(-\frac{V_{DS}}{S_f}\right)\right]$ in Eq. (8) is approaching 1. And $V_{TS} = 0$, hence, Eq. (8) may be rewritten as

$$I_{DS}^{subf} = \frac{W}{L}\cdot I_{sub0}\cdot\exp\left(\frac{V_{GS}}{S_f} + r_n V_{DS}\right) \tag{9}$$

Here

$$r_n = \frac{\varepsilon\gamma}{C_iS_f} \tag{10}$$

The second factor is again considered. Due to the weak accumulation of electrons at the front interface, the drain voltage V_{DS} can also change the profile of electrons. This can be modeled by using a fitting parameter r and can be included in the sub-threshold slope. Therefore, a relatively accurate model for the conduction at the front interface can be written as

$$I_{DS}^{subf} = \frac{W}{L}\cdot I_{sub0}\cdot\exp\left(\frac{V_{GS}}{S_f + rV_{DS}} + r_n V_{DS}\right) \tag{11}$$
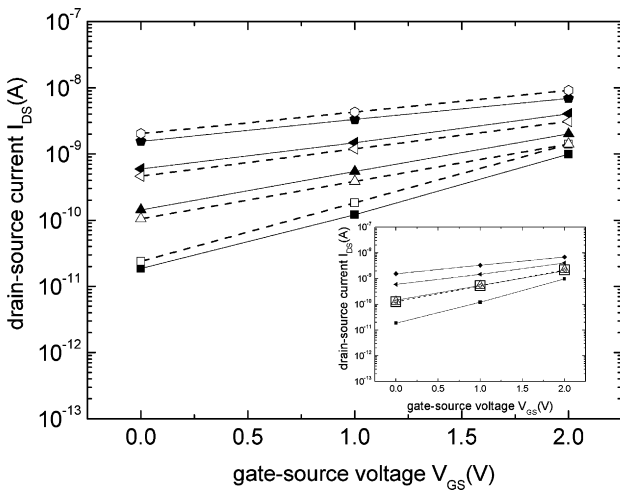

Fig. 4. Forward sub-threshold region data simulated by improved model (11). The solid markers and solid lines show the measured data; and the hollow makers and dotted lines show the simulated data. From top to bottom, $V_{DS} = 5$ V, 10 V, 15 V, 20 V, respectively. Inset: the curve of forward sub-threshold region simulated by Eq. (1).

Here, r is the fitting parameter, which embodies the effect of the weak electronic profile on the slope of the forward sub-threshold region by V_{DS}.

Fig. 4 illustrates the simulated data by Eq. (11) and the measured data in the forward sub-threshold region. The agreements between measured and simulated data by the improved models in Fig. 4 are better than those by the referenced models in the inset of Fig. 4. The models are similar to the models addressed by Khakzar et al. [4], Leroux [3], Servati [8], and Kuo [6]. In this article, the model in the forward sub-threshold region also shows the dependence on the interface quality and the material quality of a-Si:H in Refs. [8,6]. Moreover, the weak accumulation of electrons at the front interface and a lateral component of the electric field at the drain–gate overlap vicinity through V_{DS} are taken into account in the models. These can be modeled by using the fitting parameter r and r_n respectively.

The agreements between the data simulated by Eq. (11) and measured data are better on the input–output characteristics curve in Fig. 3 than those by Eq. (1) in the inset of Fig. 3. Therefore the analyses on the input–output characteristics confirm that Eq. (11) is a more model.

Using the same method in forward sub-threshold model, the reverse sub-threshold equation may be found as the following equation when a lateral component of the electric field is considered at the back interface.

$$I_{DS}^{subr} = \frac{W}{L} \cdot I_{rsub0} \cdot \exp\left(\frac{V_{GS} - V_{TR}}{S_r + r_r V_{DS}} + r_{rn} V_{DS}\right) \qquad (12)$$

Here r_r is the fitting parameter, which embodies the effect of the weak electronic profile on the slope of the reverse sub-threshold region, and r_{rn} is a lateral component of the electric field at the drain–gate overlap vicinity in virtue of V_{DS} at the back interface.

After the two factors are considered at the back interface, the agreement between the simulated data by Eq.
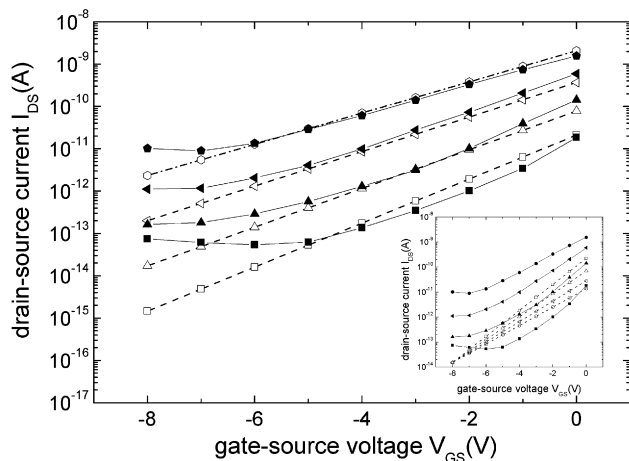

Fig. 5. Reverse sub-threshold region data simulated by improved model (12). The solid markers and solid lines show the measured data; and the hollow makers and dotted lines show the simulated data. From top to bottom, $V_{DS} = 5$ V, 10 V, 15 V, 20 V, respectively. Inset: the curve of reverse sub-threshold region simulated by Eq. (2).

Table 1
The list of process parameters and extracted parameters in modeling

Parameter			Unit
Forward sub-threshold current magnitude	I_{sub0}	2.30×10^{-12}	A
Forward sub-threshold slope	S_f	0.4871	V/dec
Forward sub-threshold fitting parameter	r	0.0559	–
Forward sub-threshold fitting parameter	r_n	0.296	V^{-1}
Reverse sub-threshold current magnitude	I_{rsub0}	5.27×10^{-17}	A
Reverse sub-threshold fitting parameter	S_r	1.6594	V/dec
Reverse sub-threshold slope	r_r	0.0229	–
Reverse sub-threshold fitting parameter	r_m	0.492	V^{-1}

(12) and the measured data is better as plotted in Fig. 5. However, the inset illustrates the simulated data by Eq. (2). The simulated data decrease as the drain–source voltage V_{DS} increases, while the measured data increase with V_{DS}. The results simulated by Eq. (2) converge into a point at $V_{GS} = V_{TR}$.

Fig. 2 shows the *I–V* characteristics simulated by Eqs. (11) and (12) in the forward and reverse sub-threshold regions, respectively. The modeling and experimental results show a good agreement. The model also embodies some physical features of the device under the process condition.

Table 1 shows the extracted parameters in modeling and process.

4. Conclusions

The model in sub-threshold region of the *I–V* curve for a-Si: H TFTs are developed in this paper. The densities of interface states at the front and back interface are similar to the values of the reference, but when the factors by virtue of V_{DS} are considered, the accuracy of simulation is improved. They can be observed from the model by fitting parameter of the weak accumulation of electrons and a lateral component of the electric field, viz. r, r_n at the front interface, and r_n, r_{rn} at the back interface, respectively. The results of using these models show a good agreement between measured and simulated data, which are superior to those used in other models. Current models can be used to evaluate and predict the electrical characteristics of TFTs, and would be helpful to the design of a-Si:H TFTs array.

References

[1] Rahn JT, Lemmi F, Lu JP, Mei P, Apte RB, Street RA, et al. High resolution X-ray imaging using amorphous silicon flat-panelarrays. IEEE Trans Nucl Sci 1999;46(3):457.
[2] Ibaraki N. a-Si TFT technologies for AM-LCDs. Mater Res Soc Symp Proc 1994;336:749.

[3] Leroux T. Static and dynamic analysis of amorphous-silicon field-effect transistors. Solid State Electron 1986;29(1):47.

[4] Khakzar K, Lueder E. Modeling of amorphous-silicon thin-film transistors for circuit simulations with SPICE. IEEE Trans Electron Dev 1992;39(6):1428.

[5] Aoki H. Dynamic characterization of a-Si TFT-LCD pixels. IEEE Trans Electron Dev 1996;43(1):31.

[6] Kuo Y. Amorphous silicon film transistors. Thin film transistors, materials and processed. 1st ed. 2004. New York: Kluwer Academic Publishers, p. 107–17.

[7] Slade HC, Shur MS, Deane SC, Hack M. Below threshold conduction in a-Si:H thin film transistors with and without a silicon nitride passivating layer. Appl Phys Lett 1996;69(17):2560.

[8] Servati P, Nathan A. Modeling of the reverse characteristics of a-Si:H TFTs. IEEE Trans Electron Dev 2002;49(5):812.

[9] Street RA, Thompson MJ. Electronic states at the hydrogenated amorphous silicon/silicon nitride interface. Appl Phys Lett 1984;45(7):769.

[10] Servati P, Nathan A. Modeling of the static and dynamic behavior of hydrogenated amorphous silicon thin-film transistors. J Vac Sci Technol A 2002;20(3):1038.

[11] Street RA, Thompson MJ, Johnson NM. The electrical characterization of surfaces, interfaces and contacts to a-Si:H. Philos Magn B 1985;51(1):1.